"Interaction of Strong Turbulence with Free Surfaces", World Scientific, Advances in Coastal and Ocean Engineering Series, Vol. 8, Singapore (ISBN 981-02-4952-7)

VERY STRONG FREE-SURFACE AERATION IN TURBULENT FLOWS: ENTRAINMENT MECHANISMS AND AIR-WATER FLOW STRUCTURE AT THE "PSEUDO" FREE SURFACE

H. CHANSON

Department of Civil Engineering
The University of Queensland
Brisbane QLD 4072, Australia

Interactions between turbulent waters and the atmosphere may lead to some air-water mixing, often called 'white water'. This study reviews the basic entrainment processes for a wide range of flow situations and presents new evidence leading to a better understanding of the basic multiphase flow dynamics. The focus is on flow situations characterised by very-strong air-water interactions: e.g., vertical plunging jet, stepped chute flow, plunging breaker. The two basic entrainment mechanisms are local and interfacial aerations. In a local aeration process, air is entrapped at the singularity/discontinuity between the impinging jet and the receiving pool of water. At low jet velocities, the bubbles are entrained individually while, at high jet impact velocities, an elongated air cavity is set into motion between the entrained fluid and the jet flow. At impingement, air is entrapped by a Couette flow mechanism. Interfacial aeration occurs when turbulent velocity fluctuations acting next to the free-surface become large enough to overcome surface tension and buoyancy. The sizes of the bubbles and droplets extend over several orders of magnitude. Void fraction distributions may be modelled by advective diffusion models. Turbulence intensity measurements suggest high levels of turbulence across the entire air-water flow, of one to two orders of magnitude greater than in monophase flows. In coastal engineering, air entrainment is characterised by unsteadiness and high levels of aeration. The results demonstrate that air entrainment in coastal and oceanic zones is an important process and cannot be ignored.

1 Introduction

The interactions between flowing waters and the atmosphere may lead to strong air-water mixing and complex multiphase flow situations. Such air-water flow mixtures are called self-aerated flows [a], free-surface aerated flows and *'white water'* [b]. The latter is the non technical term used to design the entrainment of air in turbulent flows (figure 1). The 'whitish' appearance of the flow is given by the refraction of light on the entrained air bubbles. Well-

[a] Self-aeration is called *Selbstbelüftung* in German, and *Aération, Ventilation naturelle* or *Insufflement* in French
[b] *Eau blanche* in French

known 'white water sports' include canoe, kayak and rafting racing down swift-flowing turbulent waters.

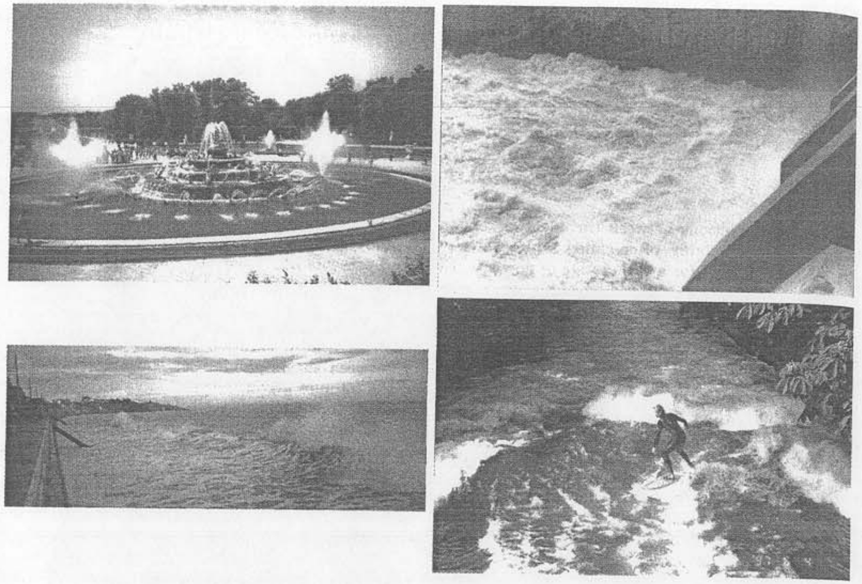

Figure 1. Interactions between strong turbulence and free-surface leading to "white water". Top left: water jets and cascading waters, Bassin de Latone, Versailles (France) in June 1998. Top right: spillway flow at La Grande 2 (Canada), flow from right to left (Courtesy of M. Lefebvre). Bottom left: wave breaking and reflection at high tide, Val-Andr (France) (Courtesy of Mrs Chanson). Bottom right: surfer on the roller of a hydraulic jump, Münich (Germany) (Courtesy of D. Young).

Man has been fascinated by white water for centuries. The Greeks, Romans, Muslims and Mughals built numerous fountains and cascades. Flowing 'white water' enhanced the perception of the sites by bringing light and captivating views (figure 1 top left). Famous examples include the Tivoli garden in Italy, Nishat Bagh in India ('Garden of Gladness'), the 'Grandes Cascades' of Rueil, Marly and Versailles (Chanson 1998). A superb design was the Chadar developed by the Mughals. The steep channel ($\alpha \sim 25°$ to $30°$) had a very-rough invert to maximise free-surface aeration and sunlight reflection (e.g. Plumptre 1993, Chanson 1997, pp. 10-11).

Air-water flows have been studied only recently, compared to basic fluid mechanics. Although early observations of 'white water' include Leonardo da Vinci (1452-1519), Wen Cheng Ming (1470-1559), and Katsushita Hokusai (1826-1833), the first successful experiments were those of Ehrenberger (1926) and later the works led by L.G. Straub (e.g. Straub and Anderson, 1958). Since the 1960s, numerous researchers studied gas entrainment in liquid flows. Most studies focused onto low void fractions ($C < 5\%$). Few research projects have been engaged in strongly-turbulent flows associated with strong free-surface aeration.

1.1 Basic definitions

Air entrainment, or free-surface aeration, is defined as the entrainment/entrapment of un-dissolved air bubbles and air pockets that are carried away within the flowing fluid. The resulting *air-water mixture* consists of both air packets within water and water droplets surrounded by air. It includes also spray, foam and complex air-water structures. *Turbulence* is a phenomenon characterised by an unpredictable motion and a broad spectrum of length scales. Turbulent flows are characterised by chaotic motion with strong mixing properties. At any point, the fluid velocity changes continuously in both magnitude and direction. The term *shear flow* characterises a flow with a velocity gradient in a direction normal to the mean flow direction and in which momentum is transferred from the region of high-velocity to that of low-velocity. The term *advective diffusion of air* (or *turbulent diffusion of air bubbles*) describes the movement of bubbles from a region of higher void fraction to one of lower air concentration caused by turbulent mixing.

There are two basic types of air entrainment process. The entrainment of air packets can be localised (also termed local aeration) or continuous along the air-water interface (figure 2). Examples of *local aeration* include air entrainment by plunging jet and at hydraulic jump (figure 1, bottom right). Air bubbles are entrained locally at the intersection of the impinging jet with the surrounding waters (figure 2 top). The intersecting perimeter is a singularity, and air is entrapped at the discontinuity between a high-velocity jet flow and the receiving pool of water. *Interfacial aeration* (or continuous aeration) is defined as the air entrainment process along an air-water interface, usually parallel to the flow direction: e.g., in chute flows (figure 1 top right, figure 2 middle). An *intermediate case* is a high-velocity water jet discharging into air. The nozzle is a singularity, characterised by a high rate of aeration, followed by some interfacial aeration downstream at the jet free-surfaces (figure 1 top left, figure 2 bottom).

It is the aim of this work to review the basic entrainment processes for a wide range of flow situations, and to present new evidence leading to a better understanding of the basic multiphase flow dynamics. The basic mechanisms of air entrapment differ substantially between local aeration and interfacial aeration. Both types of aeration are reviewed. Each case is illustrated by basic flow configurations: i.e., vertical plunging jet and stepped chute flow respectively. The structure of the air-water flows is described, and applications to coastal processes are discussed.

2 Local (singular) aeration mechanism: air entrapment at plunging jets

2.1 Flow patterns

With local (singular) aeration, air entrainment results from some discontinuity at the impingement point/perimeter: e.g., plunging water jets, hydraulic jump flows. One basic example is the vertical plunging jet (figure 2, top). At the plunge point, air may be entrapment when the impacting flow conditions exceeding a critical threshold (McKeogh 1978, Ervine et al. 1980, Cummings and Chanson 1999).

McKeogh (1978) showed first that the flow conditions at *inception of air entrainment* are functions of the jet turbulence level. For a given plunging jet configuration, the onset velocity increases with decreasing jet turbulence. For water jets, the dimensionless onset velocity may be correlated by:

$$\frac{V_e \mu}{\sigma} = 0.0109(1 + 3.375 \exp^{-80Tu}) \tag{1}$$

where V_e is the onset velocity, μ is the liquid dynamic viscosity, σ is the surface tension and Tu is the ratio of the standard deviation of the jet velocity fluctuations about the mean to the jet impact velocity (Cummings and Chanson 1999). Equation (1) is compared with experimental data obtained in large-size plunging jets in figure 3. It must be noted that the quantitative results depend critically upon the **subjective definition** of air inception and the duration of the investigation period. The writer conducted experiments in a 12−mm vertical supported jet and in a 25−mm vertical circular jet. For investigation periods ranging between 5s and 500s, the onset velocity was found to increase with decreasing investigation period by a factor of 3 to 4. Note that the onset conditions may be also affected by large roughness at the surfaces of the impinging jet (Zhu et al., 1998 [c]).

[c]Their work was conducted with thin jets ($d \approx$ 5mm) and large relative roughness: i.e.,

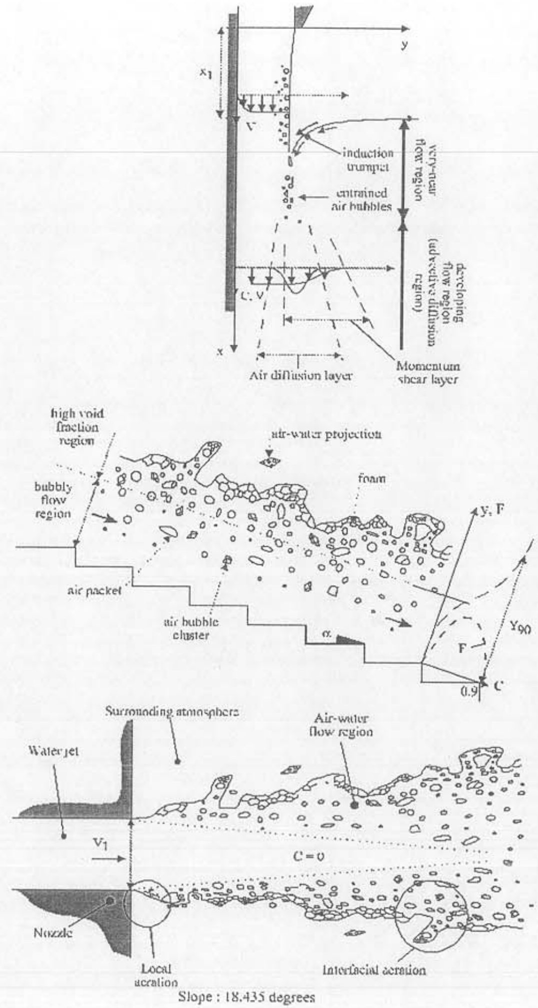

Figure 2. Sketch of basic free-surface aeration processes.

$k_s/d > 0.1$ where k_s is the equivalent roughness height and d is the circular jet diameter

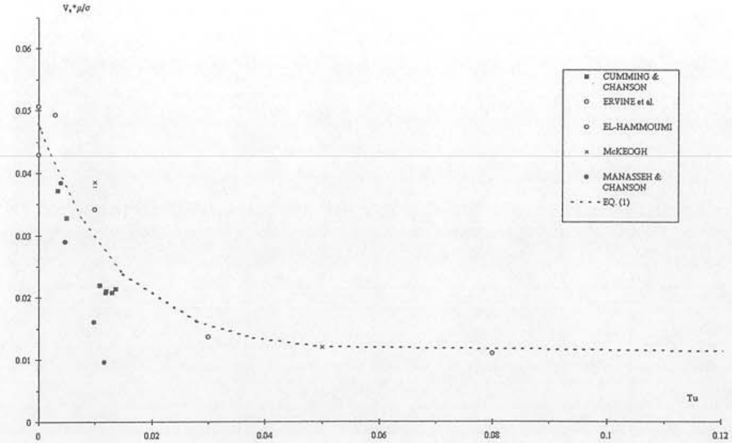

Figure 3. Onset flow conditions for air entrainment at vertical plunging jets - Comparison with equation (1) Data: McKeogh (1978), Ervine et al. (1980), El-Hammoumi (1994), Cummings and Chanson (1999), Manasseh and Chanson (2001).

For jet impact velocities slightly larger than the onset velocity, air is entrained in the form of *individual bubbles and packets*. The entrained air may have the form of 'kidney-shaped' bubbles which may break up into two 'daughter' bubbles, 'S-shape' packets, or elongated 'fingers' that may break-up to form several small bubbles by a tip-streaming mechanism, depending upon the initial size of the entrained air packet (Cummings and Chanson, 1999). The air entrainment rate is very small, hardly measurable with intrusive probes.

At higher impact velocities, the amount of entrained air becomes significant and the air diffusion layer is clearly marked by the *white plume* generated by the entrained bubbles. Air entrainment is an unsteady, rapidly-varied process. An *air cavity is set into motion* between the impinging jet and the surrounding fluid and it is stretched by turbulent shear (figure 4) (Chanson, 1997). The air cavity behaves as a ventilated air sheet and air pockets are entrained by discontinuous gusts at the lower tip of the elongated air cavity. Initial aeration of the impinging jet free-surface may further enhance the process (Van de Sande and Smith, 1973; Brattberg and Chanson, 1998).

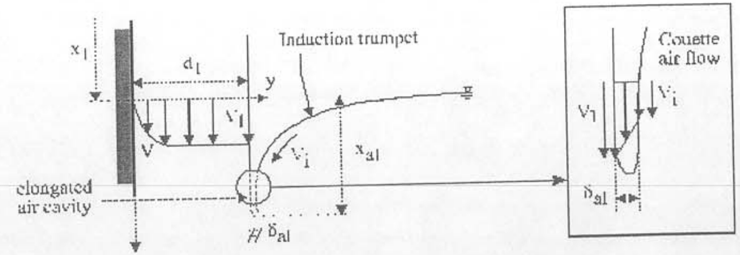

Figure 4. Detail of the air entrapment region and the very-near flow field.

2.2 *The entrapment region (or very-near flow field)*

In the very-near flow field, the flow is dominated by air entrapment and the interactions between gas and liquid entrainment (figure 4). Dominant flow features include an *induction trumpet* generated by the liquid entrainment and the *elongated air cavity* at jet impingement (thickness δ_{al}). The very-near flow region extends for about $(x - x_1)/d_1 < 5$, where $(x - x_1)$ is the depth below the free-surface and d_1 is the jet thickness at impact (figures 2 and 4). Detailed measurements were conducted in a vertical supported jet with inflow velocity ranging from 2 to 4 m/s (table 1). Air-water flow measurements were performed with hot-film and resistivity probes (Chanson and Brattberg, 1998).

Experimental observations showed that the air entrapment/entrainment process is very dynamic and it interacts substantially with the transfer of momentum across the mixing layer. Although the void fraction and mean velocity distributions exhibit smooth shapes, instantaneous velocity measurements showed a highly unstable air-water mixing layer. The shape and position of the elongated air cavity evolve very rapidly with time, and there is a **distinct velocity discontinuity** between the impinging jet flow and the induction trumpet. Such a discontinuity is sketched in figure 4 which shows an instantaneous 'snapshot' of the entrapment region. Experimental data, summarised in table 1, indicate a velocity discontinuity across the elongated air cavity: $V_i \propto (V_1 - V_e)^{0.15}$, where V_1 is the jet impact velocity and V_i is the liquid entrainment velocity (in the induction trumpet).

The writer hypothesises that air entrainment takes place predominantly in the elongated cavity by a Couette flow motion (figure 4, right). The amount of entrained air q_{air} may be estimated as :

$$q_{air} = \int_{d_1}^{d_1+\delta_{al}} V_{air}\, dy \approx \frac{V_1 + V_i}{2} \delta_{al} \qquad (2)$$

Equation (2) compares favourably with entrained air flux measured below the free-surface in table 1, columns 8 and 7 respectively. (The air flux data were recorded by Brattberg and Chanson, 1998). The close agreement between Equation (2) and data confirms the basic entrainment mechanism.

Discussion

Some researchers (Lezzi and Prosperetti, 1991; Bonetto et al., 1994) proposed various theoretical models of the air entrainment process by elongated air cavity. These however do not agree with experimental observations of the very-near flow field (table 1). It is believed that the erroneous results reflect a lack of understanding of the basic entrapment mechanisms and of the interactions between turbulent shear and entrained bubbles.

Run (1)	d_1 m (2)	V_1 m/s (3)	V_i m/s (4)	δ_{al} m (5)	$(q_{air}/q)_1$ Pre-entrain. (6)	q_{air}/q (7)	q_{air}/q Calc. eq.(2) (8)
HF-2	0.009	2	0.65	0.0015	0.11	-	0.11
HF-3	0.011	3	0.76	0.0020	0.14	0.13	0.11
HF-3	0.0116	4	0.76	0.0030	0.17	0.27	0.16

Table 1. Experimental observations of the entrapment region at a vertical supported jet. Notes: V_i: induction trumpet velocity; $(q_{air}/q)_1$: free-surface aeration of the falling jet (or pre-entrainment); each data is the average of three cross-sectional profiles.

2.3 Advective diffusion

Downstream of the entrapment region (i.e. $(x-x_1)/d_1 > 5$), the distributions of void fractions exhibit smooth, derivative profiles (figure 5). For a wide range of flow conditions ($2 < V_1 < 9$ m/s) and jet geometry, the data may be fitted by simple analytical solutions of the advective diffusion equation for air bubbles (Chanson, 1997). For two-dimensional vertical jets, it yields:

$$C = \frac{\frac{q_{air}}{q}}{\sqrt{4\pi D^{\#} \frac{x-x_1}{Y_{C_{max}}}}} \left\{ \exp\left[-\frac{\left(\frac{y}{Y_{C_{max}}} - 1\right)^2}{4D^{\#}\frac{x-x_1}{Y_{C_{max}}}} \right] + \exp\left[-\frac{\left(\frac{y}{Y_{C_{max}}} + 1\right)^2}{4D^{\#}\frac{x-x_1}{Y_{C_{max}}}} \right] \right\} \qquad (3)$$

where $D^{\#}$ is a dimensionless air bubble diffusivity and $Y_{C_{max}} = y(C = C_{max})$ (Cummings and Chanson, 1997). Cummings and Chanson (1997b) and Brattberg and Chanson (1998) presented successful comparisons between equation (3) and experimental data.

With circular plunging jets, the analytical solution of the diffusion equation becomes:

$$C = \frac{q_{air}}{q} \frac{1}{4D^{\#}\frac{x-x_1}{Y_{C_{max}}}} \exp\left[-\frac{1}{4D^{\#}} \frac{\left(\frac{r}{Y_{C_{max}}}\right)^2 + 1}{\frac{x-x_1}{Y_{C_{max}}}} \right] I_0\left[\frac{1}{2D^{\#}} \frac{\frac{r}{Y_{C_{max}}}}{\frac{x-x_1}{Y_{C_{max}}}} \right] \qquad (4)$$

where I_0 is the modified Bessel function of the first kind of order zero. In figure 5, equation (4) is compared with experimental data obtained in a 25-mm diameter vertical plunging jet.

Figure 5 shows also dimensionless distributions of bubble count rate, where the bubble count rate F is defined as the number of bubbles impacting the probe tip per second. For a given void fraction and velocity, the bubble count rate is inversely proportional to the (number) mean bubble diameter and directly proportional to the air-water specific interface area. Figure 5 illustrates that the maximum bubble count rate occurs in the inner jet region: i.e., at a distance from the jet centreline that is smaller than the location $Y_{C_{max}}$ where the void fraction is maximum. The result is observed consistently with both two-dimensional and circular plunging jets (Brattberg and Chanson, 1998; Present study). It highlights that the relationship between void fraction and bubble count rate is not unique in plunging jet flows. Brattberg and Chanson (1998) assumed that the result was caused by *"the non-coincidence between the air bubble diffusion layer and the momentum shear layer"*, shown by Cummings and Chanson (1997b) and Brattberg and Chanson (1998) in two-dimensional jets.

3 Interfacial aeration process : self-aeration down a stepped cascade

3.1 Introduction

Examples of interfacial aeration include spillway flows and 'white water' down a mountain stream (figure 1 and 6). One case, the cascading waters down a stepped chute, is characterised by very-energetic turbulence and free-surface aeration (figure 6, bottom). Considering a given stepped geometry, low flows behave as a succession of free-falling nappes (called *nappe flow regime*), and little aeration is observed. With increasing flow rates, a *transition flow regime*

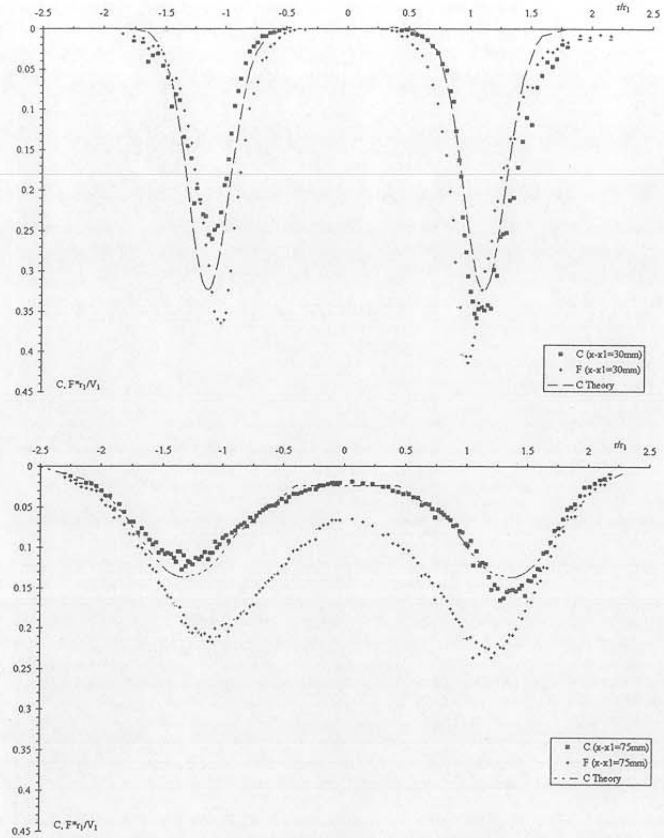

Figure 5. Void fraction distributions at a circular plunging jet - Comparison with equation (4)) $d_1 = 0.024$ m, $V_1 = 5.3$ m, $x_1 = 0.2$ m, $Tu = 0.8\%$ (at impact). Top: $(x - x_1) = 30$ mm - Bottom: $(x - x1) = 75$ mm.

occurs at intermediate discharges. Dominant flow features included strong splashing and droplet ejections. For an observer standing on the bank, the transition flow has a chaotic appearance with irregular droplet ejections that are seen to reach heights of up to 3 to 5 times the step height. At larger flow rates, the waters skim over the pseudo-bottom formed by the step edges: i.e., *skimming flow regime* (figure 6, bottom). Intense cavity recirculation is

observed and the flow resistance is form drag predominantly.

In both transition and skimming flows, the upstream flow is non-aerated but free-surface instabilities are observed. Similar wave instability were discussed by Anwar (1993) and Chanson (1997). The location of the inception of free-surface aeration is clearly defined however (figure 6, bottom). Downstream the flow becomes rapidly aerated. At Trigomil dam, the chute sidewalls were overtopped during the flood event. In this section, the stepped chute flow is used to illustrate the complex interactions between strong turbulence and interfacial aeration. The discussion is based upon new experimental results obtained in a large-size stepped chute: i.e., 1 m wide, 3 m long, 0.1 m high steps, 21.8° mean invert slope and flow rates up to 300 l/s.

3.2 Definition of the 'free-surface'

Keulegan and Patterson (1940) analysed wave instability and implied that air bubbles may be entrained by a breaking wave mechanism at the free surface. Photographs by Cain (1978) at Aviemore dam spillway showed that air is entrained by the action of a multitude of irregular vortices acting next to the free-surface. Basically air bubble entrainment is caused by turbulence fluctuations acting next to the air-water free surface. Through this interface, air is continuously trapped and released. Air bubble may be entrained when the turbulent kinetic energy is large enough to overcome both surface tension and gravity effects. The turbulent velocity be greater than the surface tension pressure and the bubble rise velocity component for the bubbles to be carried away:

$$v' > \text{Maximum}\left(\sqrt{\frac{8\sigma}{\rho d_{ab}}}\,;u_r\cos\alpha\right) \tag{5}$$

where v' is an instantaneous turbulent velocity normal to the flow direction, σ is the surface tension, ρ is the water density, d_{ab} is the diameter of the entrained bubble, u_r is the bubble rise velocity and α is the channel slope (Ervine and Falvey, 1987; Chanson, 1993). Equation (5) predicts the occurrence of air bubble entrainment for $v' > 0.1$ to 0.3 m/s. The condition is nearly always achieved in stepped chute flows because of the strong turbulence generated by the stepped invert (see section 3.5).

Interfacial aeration involves both the entrainment of air bubbles and the formation of water droplets. When free-surface aeration takes place, the exact location of the interface between the flowing fluid and the above atmosphere becomes undetermined (figure 6). There is however continuous exchanges of air-water and of momentum between the flowing waters and the atmosphere.

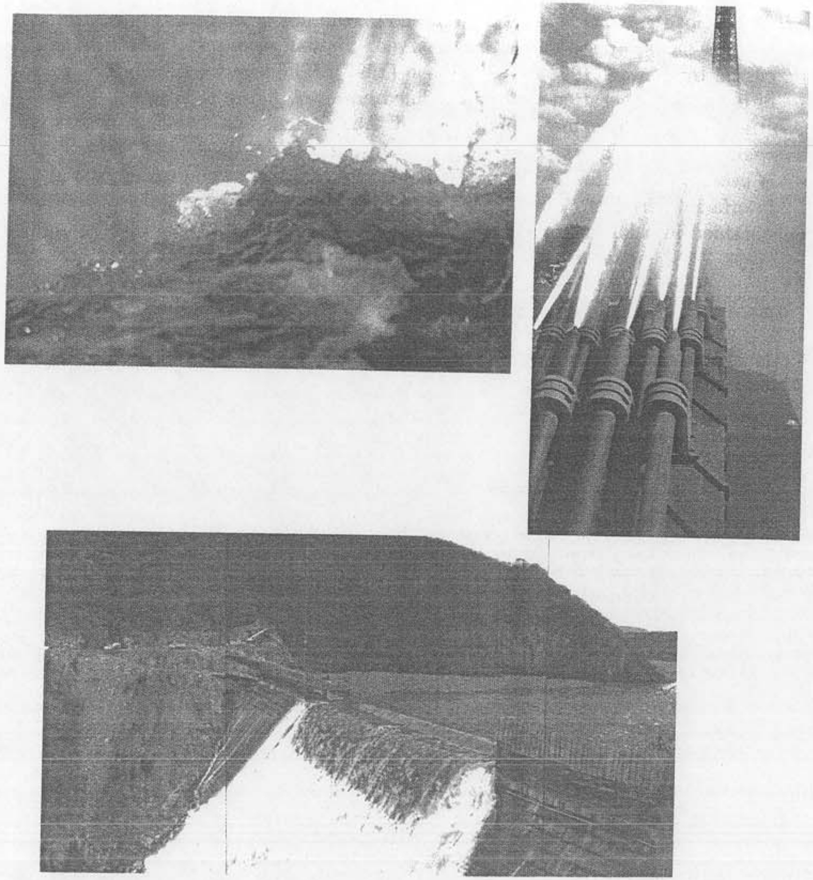

Figure 6. Photographs of air-water interfacial flow features. Top left: water droplet ejections at Iguazu Falls (Argentina) (Courtesy of Dr R. Manasseh). Top right: water cannons at Jardins du Trocadro (France) (Courtesy of Mrs Chanson) - There are 20 water guns with jet lengths of 50 m and maximum height of 15 m. Bottom: skimming flow down Trigomil stepped spillway (Mexico): $Q = 1,017$ m^3/s, chute width: 75 m (Courtesy of Drs Sanchez-Bribiesca and Gonzales-Villareal).

The writer defines the *interface between the air-water mixture flow and the atmosphere* as the iso-void fraction line $C = 90\%$. Model and prototype data showed that the air-water flow behaves as a homogeneous mixture for $C < 0.90$ with smooth, continuous distributions of void fraction, air-water velocity and bubble count rate (Wood, 1991; Chanson, 1997). For larger void fractions (i.e. $C > 90\%$), the air-water-mixture is a fine spray, sometimes behaving as a series of free-fall particles (figure 6, left).

The air-water mixture consists of water surrounding air bubbles ($C < 30\%$), air surrounding water droplets ($C > 70\%$) and an intermediate flow structure for $0.3 < C < 0.7$ (figure 2). In regions of low air contents ($C < 0.3$) the flow has a *bubbly mixture* appearance. At larger air contents ($C > 0.3$), the multiphase flow structure becomes more complex with several types of air-water structures: e.g., air-water projections, foam. Rein (1998) and Chanson (1999) discussed specifically the spray region (i.e. $C > 95\%$). Waves and wavelets propagate also downstream along the free-surface ([d].). A phase detection probe, fixed in space, will record a fluctuating signal corresponding to both air-water structures and wave passages, adding complexity of the interpretation of the signal (Toombes, 2002).

3.3 Advective diffusion of air bubbles

Downstream of the inception point of free-surface aeration, air and water are fully mixed, forming a homogeneous two-phase flow (Chanson, 1995; 1997). The advective diffusion of air bubbles may be described by simple analytical models (Appendix I). In transition flows, the distributions of void fraction follow closely:

$$C = K' \left[1 - \exp\left(-\lambda \frac{y}{Y_{90}}\right)\right] \qquad \text{Transition flows} \qquad (6)$$

where y is the distance measured normal to the pseudo-invert, Y_{90} is the characteristic distance where $C = 90\%$, K' and λ are dimensionless functions of the mean air content only. Equation (6) compares favourably with experimental data (figure 7 top) but for the first step edge downstream of the inception point of free-surface aeration and for the deflecting jet flow.

[d]Most aerated chute flows are supercritical and wavelets can only propagate into the downstream direction

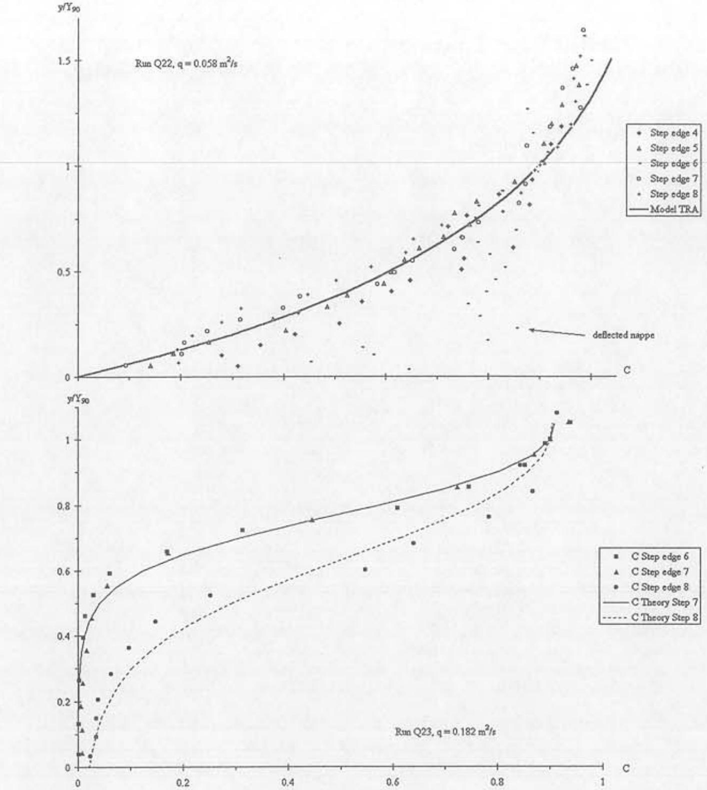

Figure 7. Dimensionless distributions of void fraction in stepped chute flow ($\alpha = 21.8°$, step height: 0.1 m, chute width: 1 m). Top: Transition flow, $q = 0.058$ m^2/s (data measured at outer step edges) - Comparison with Equation (6). Bottom: skimming flow, $q = 0.182$ m^2/s (data measured at outer step edges) - Comparison with equation (7).

In skimming flows, the air concentration profiles may be modelled by:

$$C = 1 - \tanh^2\left[K' - \frac{\frac{y}{Y_{90}}}{2D_0} + \frac{\left(\frac{y}{Y_{90}} - \frac{1}{3}\right)^3}{3D_0}\right] \quad \text{Skimming flows} \quad (7)$$

where K' is an integration constant and D_0 is a function of the mean void fraction only. In figure 7 (bottom), laboratory data are compared successfully with equation (7). Although figure 7 highlights different shapes of void fraction distribution between transition and skimming flows, equations (6) and (7) derive from the same basic equation assuming different diffusivity profiles (Appendix I).

Figure 8 presents dimensionless distributions of bubble count rates Fd_c/V_c, where d_c is the critical depth and V_c is the critical flow velocity. The data are compared with a parabolic shape. The results show that the relationship between the bubble frequency and void fraction is unique, in both transition and skimming flows. Toombes (2002) demonstrated the unicity of the relationship and he proposed a sophisticated model comparing favourably with experimental data obtained in water jets discharging into air, smooth-chute flows and stepped chute flows (e.g. Brattberg et al., 1998; Chanson, 1997b; Present study).

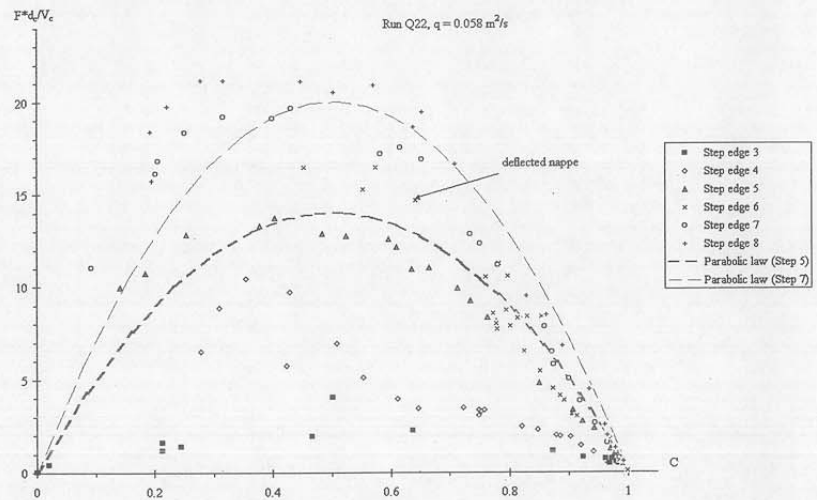

Figure 8. Dimensionless bubble count rate distributions in stepped chute flow ($\alpha = 21.8°$, step height: 0.1 m, chute width: 1 m) - Transition flow, $q = 0.058$ m^2/s.

3.4 Characteristic bubble/droplet sizes

Details of the air-water flow structure may be gained from bubble and droplet size measurements. Figures 9 and 10 present normalised chord length probability distribution functions. (Measurements were conducted with a fine resistivity probe (25 µm ∅ sensor).) In figures 9 and 10, each histogram column represents the probability of a bubble/droplet chord length in 0.5 mm intervals: e.g., the probability of a chord length from 2.0 to 2.5 mm is represented by the column labelled 2.0. The last column (i.e. > 20) indicates the probability of bubble/droplet chord lengths larger than 20 mm. Figure 9 presents data obtained in a transition flow for the same flow rate as in figures 7 (top) and 8. Figure 10 shows skimming flow data for the same discharge as in figure 7 (bottom).

The results show a broad spectrum of bubble and droplet chord lengths at each location: i.e., from less than 0.5 mm to larger than 20 mm (figures 9 and 10). The chord length distributions are typically skewed with a preponderance of small bubble/droplet sizes relative to the mean. The probability of air *bubble chord lengths* is the largest for bubble sizes between 0 and 1.5 mm for $C \approx 0.1$ and between 0 and 2.5 mm for $C \approx 0.2$. It is worth noting the amount of bubbles larger than 20 mm for $C \approx 0.2$ in skimming flows. These might be large air packets surrounding water structures. Although *water droplet chord length distributions* appear skewed with a preponderance of small drop sizes relative to the mean, the distributions differ from bubble chord length distributions for similar liquid and void fractions respectively. For a given void/liquid fraction, the droplet chord mode and mean are larger than the corresponding bubble chord length data (figures 9 and 10).

3.5 Turbulent velocity field

Air-water velocity distributions are presented in Figure 10 in terms of the time-averaged air-water velocity V and a modified turbulence intensity Tu'. The data were measured with a dual-tip resistivity probe and details of the processing technique are given in Appendix II. Although Tu' is not exactly equal to the turbulence intensity, it provides some qualitative information on the turbulence level in the flow. Figures 11 and 12 include transition and skimming flow data for the same flow conditions as in figures 7, 8, 9 and 10. The velocity data compare favourably with a power law in skimming flows (figure 12). In figures 11 and 12, the distributions of turbulence intensity Tu' exhibit relatively uniform profiles implying high turbulence levels across the entire air-water flow mixture (i.e. $0 \leq y \leq Y_{90}$). The trend is observed in both skimming and transition flows, and it differs significantly

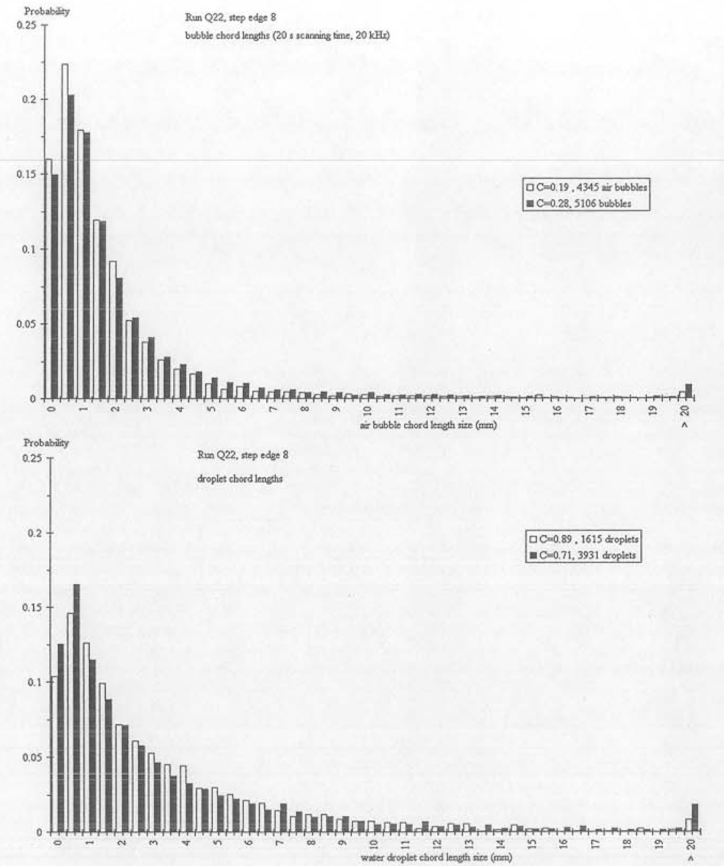

Figure 9. Bubble and droplet chord length distributions (measured at Step edge 8). Transition flow: $q = 0.058$ m^2/s - Top: air bubble chord lengths - Bottom: droplet chord lengths.

from well-known turbulence intensity profiles observed in turbulent boundary layers (e.g. Schlichting, 1979). It is believed that, on stepped chutes, the high rate of energy dissipation, associated with form drag generated by the steps, contributes to strong turbulent mixing throughout the entire flow. Although

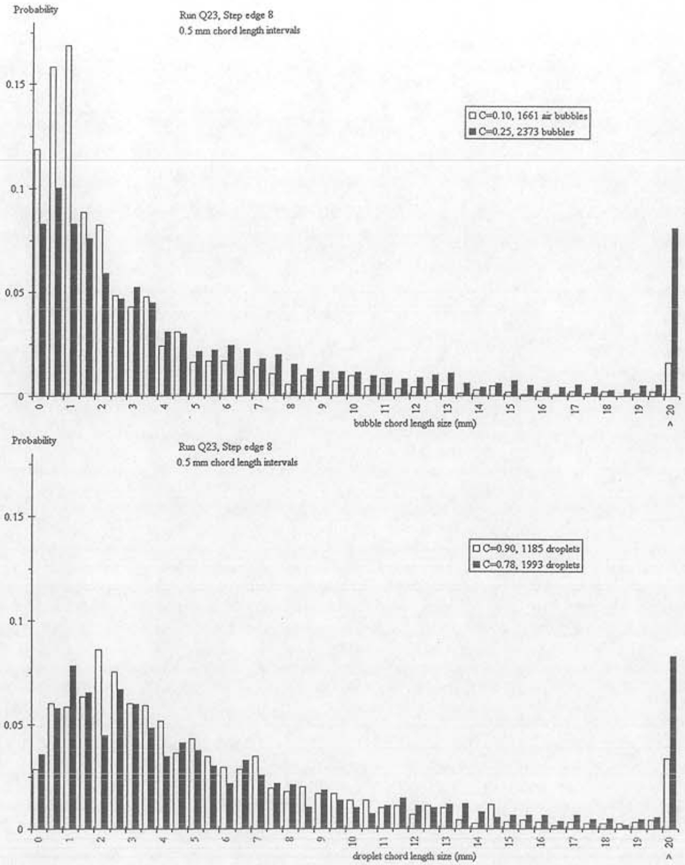

Figure 10. Bubble and droplet chord length distributions (measured at Step edge 8). Skimming flow: $q = 0.182$ m^2/s - Top: air bubble chord lengths - Bottom: droplet chord lengths.

the quantitative values of turbulence intensity Tu' are large ($\sim 100\%$), they are of the same order of magnitude as turbulence levels measured in the developing shear region of plunging water jets with hot-film probes (Chanson and Brattberg, 1998).

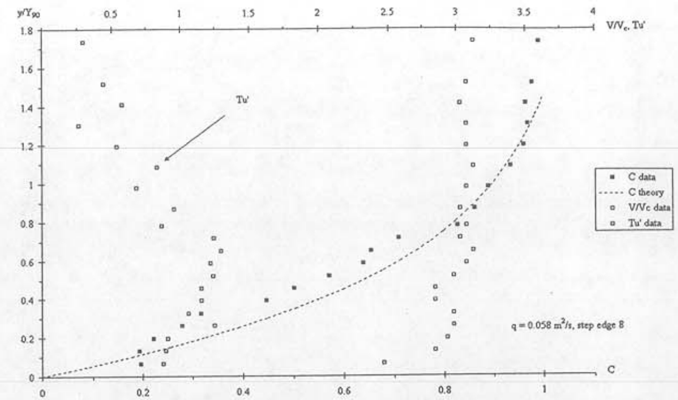

Figure 11. Dimensionless velocity and turbulent intensity distributions (measured at Step edge 8). Transition flow: $q = 0.058$ m^2/s.

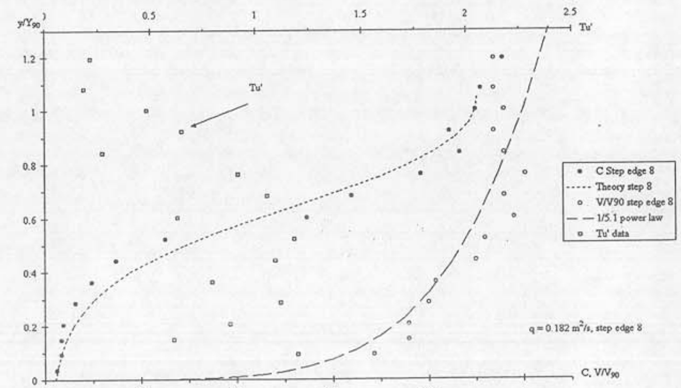

Figure 12. Dimensionless velocity and turbulent intensity distributions (measured at Step edge 8). Skimming flow: $q = 0.182$ m^2/s.

4 Applications to coastal processes: unsteady air entrainment at plunging breakers

4.1 Presentation

In oceanic and coastal regions, air bubble entrainment by breaking waves is a significant factor under high wave conditions. A dominant feature is the unsteadiness of the process and the widespread surface area of 'white capping' during storm (figure 13). Air bubble entrainment at breaking waves contributes significantly to air-sea mass transfer because the net surface area of thousands of tiny bubbles is much greater than the surface area above the bubble clouds. This is an important process for the exchange of nitrogen, oxygen and carbon dioxide between atmosphere and oceans. One type of breakers, the plunging breaking wave, has the potential to entrain a very large amount of air bubbles at great depths. At a plunging breaker, bubble entrainment is caused by the top of the wave forming a water jet projecting ahead of the wave face and entraining air when it impacts the water free-surface in front of the wave. In shallow water, the plunging breaking process is affected by the sloping bottom but air bubble entrainment is still significant.

Figure 13. Air entrainment at breaking waves on the Enshu coast, Japan on 21 Jan. 2001 with a strong wind parallel to the beach.

The entrained bubbles induce firstly a rise in water level associated with an energy transfer into potential energy while breaker-generated waves propagate in off-and-onshore directions (e.g. Fuhrboter, 1970). However the influence of entrained air on the wave field near the surf zone has not been well investigated except for some research on energy dissipation by wave breaking. The air bubble entrainment process is improperly scaled by a Froude similitude (Wood, 1991; Chanson, 1997) and most laboratory experiments tend to underestimate its effects. In the following paragraphs, the unsteady air entrainment process at a plunging breaker is discussed based upon near-full-scale work conducted by Chanson et al. (1999; 2000) ([e]).

4.2 Unsteady air-water flow patterns

The initial jet impact was associated with *strong splashing* of short duration (i.e. less than 0.4 s) and the generation of a downward underwater bubble plume. The splashing was characterised by small liquid fractions (i.e. < 2%) and some droplets travelled up to 2.5−m from the impact point and reached heights in excess of 0.4 m above the initial free-surface level. A similar splashing process was observed, in field and laboratory, during the initial stage of the plunging breaking wave (e.g. Tulin and Waseda, 1999).

Below the free-surface, the initial bubble entrainment formed a densely populated *'bubble plume'* travelling downwards until it reached the bottom and then propagated parallel to the bed with clear-water above as the plume front expanded with rising bubbles (figure 14). The mechanism was of short duration (< 1 sec. for 0.4 m water depth) and the plume travelled horizontally up to $x/d = 3$, where d is the initial water depth. Slow motion pictures suggested that the celerity of bubble plume front was about 30 to 45% of the jet impact velocity during both the downward and horizontal motions. Figure 14 presents two underwater photographs of the horizontal propagation of the bubbly plume toward the camera.

This rapid sequence of events was followed by the development of a *'boiling' flow* next to the plunge point. This region was extremely turbulent with a lot of entrained air bubbles and it had the same appearance as a hydraulic jump roller. The roller/boiling flow pattern lasted typically 50% longer than the plunging jet. Visually most entrained air bubbles disappeared after about

[e] The plunging jet of the breaker was modelled by an unsteady water jet (0.75−m by 0.07−m) discharging into a wave flume with initial depths ranging from 0.2 to 0.5m. For some experiments, air entrainment was suppressed (by a factor of 2 to 3) to investigate specifically the effects of air entrainment at breaking. The model only simulates part of the breaker since it does not have a horizontal velocity relative to the still water

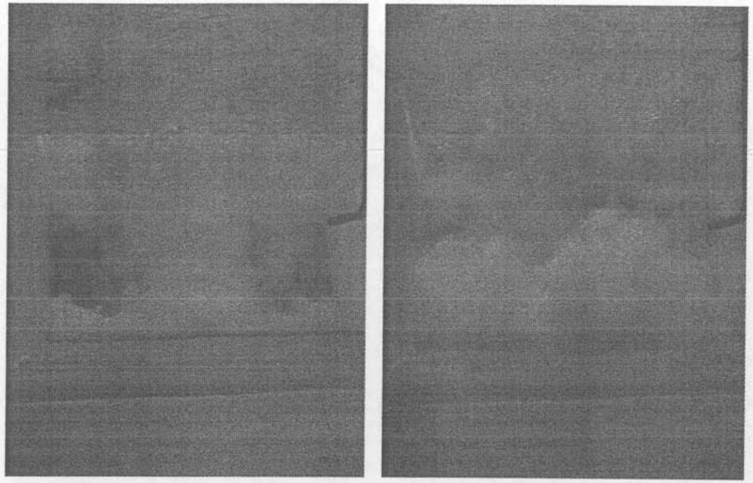

Figure 14. Underwater 'bubble plume' during the initial phase of a plunging breaker, looking toward the jet impact - Initial water depth: 0.40 m, initial breaker volume: 0.628 m^3, initial head: 1.374 m, initial impact velocity: 5.2 m/s. Left: 0.367 sec. after nappe impact. Right: 0.50 sec. after nappe impact.

3 to 4 times the breaker duration, although fine bubbles were still seen several minutes after the experiment end.

Shortly after nappe impact, a positive surge propagated into the wave flume. When air entrainment was suppressed, the free-surface levels, measured at several locations along the flume, were in close agreement with theoretical results deduced from the continuity and momentum principles, and from the equations of Saint-Venant (Chanson et al., 1999).

4.3 Effects of air entrainment

At a plunging breaker, a significant flow bulking (i.e. water level rise) was observed next to the nappe impact; the water level data were consistently higher than theoretical predictions. The differences implied an average void fraction of nearly 12% next to the nappe impact and about 4 to 6% at about 1 m downstream of the nappe impact for the duration of the breaker (figure

15). The impact on the water level rise is the greatest in shallow waters while the contribution to air-sea mass transfer is maximum in deep waters.

The wave data analysis suggested further that air entrainment affected the wave field, in particular the more energetic waves. Higher water levels were observed in the early stages, followed by lower water levels. The initial water level rise was caused by the entrained bubbles while the subsequent drop in water level was induced by a strong circulation associated with the upwelling current due to bubble rise, the time scale of which was almost linear to the water depth (i.e. the rise time of the bubbles).

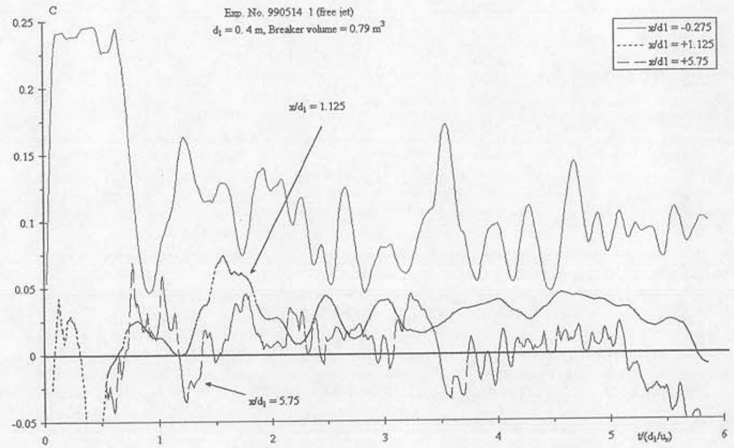

Figure 15. Fluctuations of the depth-averaged void fraction at three longitudinal locations next to a plunging breaker - Initial water depth: 0.40 m, initial breaker volume: 0.79 m^3, breaker duration: $6.9d_1/u_r$ ($u_r = 0.2$ m/s).

4.4 Discussion

Wave breaking near the coastline is often associated with significant sediment transport and the resulting flow becomes a three-phase flow: gas (air), liquid (water) and solid (sediment). The challenges ahead of fluid dynamics experts will be to comprehend the interactions between the three phases. In this case study, physical modelling was conducted in a large-size facility because the breaking process cannot be modelled analytically nor numerically in a simple manner. In laboratory, the flow parameters can be controlled but the selection of the model scale is critical to minimise scale effects. For example, in the field, a 0.2–m high breaking wave will be characterised by some air entrainment while a 1 : 4 scale model of the same wave will not. It must be emphasised that the study modelled incompletely a plunging breaker since the plunging jet a horizontal velocity component.

5 Summary and Recommendations

In Nature, strong turbulence acting next to a free-surface is often characterised by free-surface aeration and 'white water'. There are two basic mechanisms of air bubble entrainment: local (singular) aeration and interfacial aeration. Both are reviewed in situations where the void fractions and turbulence levels are very-significant.

In a local aeration process, air is entrapped at the singularity (discontinuity) between the impinging jet and the receiving pool of water. At low jet velocities, the bubbles are entrained individually and the entrained air packets may subsequently be broken up into smaller bubbles by turbulent shear. At high jet impact velocities, an elongated air cavity is set into motion between the entrained fluid and the jet flow. Air is entrapped into a Couette flow motion. Downstream, the distribution of air bubbles may be predicted accurately with simple advective diffusion models.

Interfacial aeration occurs when turbulent velocity fluctuations acting next to the free-surface become large enough to overcome surface tension and buoyancy. One extreme case, the stepped cascade flow, is characterised by strong turbulence and aeration. The sizes of the bubbles and droplets extend over several orders of magnitude. Chord length distributions are typically skewed with a preponderance of small bubble/droplet sizes relative to the mean, but droplet and bubble size distributions have different shapes for identical liquid and void fractions respectively. Void fraction distributions may be modelled by advective diffusion models. Turbulence intensity measurements suggest high levels of turbulence across the entire air-water flow, with a magnitude greater than in monophase flows.

In coastal engineering, air entrainment is characterised by unsteadiness. A large size experiment showed new air-water flow features and high levels of aeration. The results demonstrate that air entrainment in the surf zone is an important process and it cannot be ignored.

Acknowledgments

The writer thanks Dr S. Aoki, Ms Y.H. Chou, Dr R. Manasseh, Dr L. Toombes, for their help and assistance. He further acknowledges the assistance of his students B. Bolden, T. Brattberg, M. Eastman, T. McGibbon, M. Maruyama, N. Van Schagen.

Appendix I - Air bubble diffusion in self-aerated chute flows

In supercritical flows, 'white water' occur when turbulence acting next to the free-surface is large enough to overcome both surface tension for the entrainment of air bubbles and buoyancy to carry downwards the bubbles. Assuming a homogeneous air-water mixture for $C < 90\%$, the advective diffusion of air bubbles may be analytically predicted. At uniform equilibrium, the continuity equation for air in the air-water flow yields:

$$\frac{\partial}{\partial y}\left(D_t \frac{\partial C}{\partial y}\right) = \cos\alpha \frac{\partial}{\partial y}(u_r C) \tag{I.1}$$

where D_t is the turbulent diffusivity, u_r is the bubble rise velocity, α is the channel slope and y is measured perpendicular to the mean flow direction. In a fluid of density $\rho(1 - C)$, the bubble rise velocity equals:

$$u_r^2 = \left[(u_r)_{Hyd}\right]^2 (1 - C) \tag{I.2}$$

where $(u_r)_{Hyd}$ is the rise velocity in a hydrostatic pressure gradient. A first integration of the continuity equation for air in the equilibrium flow region leads to:

$$\frac{\partial C}{\partial y'} = \frac{1}{D'} C\sqrt{1 - C} \tag{I.3}$$

where $y' = y/Y_{90}$ and D' is a dimensionless turbulent diffusivity.

Assuming a homogeneous turbulence across the flow (i.e. D' constant), Chanson (1995; 1997) obtained:

$$C = 1 - \tanh^2\left(K' - \frac{y'}{2D'}\right) \tag{I.4}$$

where K' is an integration constant. Equation (I.4) was shown to fit well model and prototype data (Chanson, 1995).

More refined models of void fraction distributions may be developed assuming a non constant diffusivity (equations (6) and (7)). In transition flows, experimental data are best fitted by equation (6) assuming:

$$D^{'} = \frac{C\sqrt{1-C}}{\lambda(K' - C)}. \tag{I.5}$$

In skimming flows, the following diffusivity profile provides a good agreement with data (equation (7)):

$$D^{'} = \frac{D_0}{1 - 2\left(\frac{y}{Y_{90}} - \frac{1}{3}\right)^2}. \tag{I.6}$$

Appendix II - Velocity measurements and cross-correlation techniques for dual-tip probe measurements in gas-liquid flows

In turbulent gas-liquid flows, a velocity measurement technique is based upon the successive detection of bubbles/droplets by two sensors: i.e., double tip optical and resistivity probes (figure II.1). The technique assumes that:

1. the probe sensors are aligned along a streamline,
2. the bubble/droplet characteristics are little affected by the leading tip, and
3. the bubble/impact impact on the trailing tip is similar to that on the leading tip.

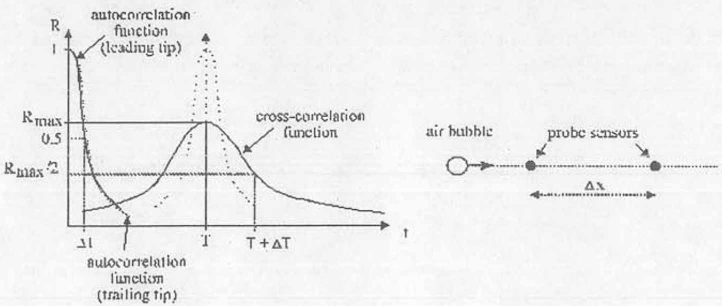

Figure II.1. Sketch of a cross-correlation function and dual-tip probe.

In highly turbulent gas-liquid flows, the successive detection of a bubble by each probe sensor is highly improbable, and it is common to use a cross-correlation technique (e.g. Crowe et al., 1998, pp. 309-318). The average air-water velocity is defined as:

$$V = \frac{\Delta x}{T} \tag{II.1}$$

where Δx is the distance between probe sensors and T is the travel time for which the cross-correlation function is maximum: i.e., $R(T) = R_{max}$ where R is the normalised cross-correlation function and R_{max} is the maximum cross-correlation value (figure II.1).

The shape of the cross-correlation function provides a further information on the turbulent velocity fluctuations. Flat cross-correlation functions are associated with large velocity fluctuations around the mean and hence large turbulence intensity $Tu = u^{'}/V$, where $u^{'}$ is the standard deviation of the turbulent velocity fluctuations. Thin high cross-correlation curves are characteristics of small turbulent velocity fluctuations. The information must be corrected to account for the intrinsic noise of the leading probe signal and the turbulence intensity is related to the broadening of the cross-correlation function compared to the autocorrelation function (figure II.1).

The definition of the standard deviation of the velocity leads to:

$$u^{'2} = \frac{V^2}{N}\sum_{i=1}^{N}\frac{1}{t^2}(t-T)^2 \tag{II.2}$$

where V is the mean velocity, N is the number of samples and t is the bubble travel time data. With an infinitely large number of data points N, an extension of the mean value theorem for definite integrals may be used as the functions $1/t^2$ and $(t-T)^2$ are positive and continuous over the interval $[i = 1, N]$ (Spiegel, 1974). It implies that there exists at least one characteristic bubble travel time $t^{'}$ satisfying $t_1 \le t^{'} \le t_N$ such that:

$$\left(\frac{u^{'}}{V}\right)^2 = \frac{1}{N}\frac{1}{t'^2}\sum_{i=1}^{N}(t-T)^2. \tag{II.3}$$

That is, the standard deviation of the velocity is proportional to the standard deviation of the bubble travel time:

$$\frac{u^{'}}{V} = \frac{\sigma_t}{t^{'}}. \tag{II.4}$$

Assuming that the successive detections of bubbles by the probe sensors is a true random process ([f]), the cross-correlation function would be a Gaussian distribution:

$$R(t) = R_{max} \exp\left[-\left(\frac{t-T}{\sigma_T}\right)^2\right] \tag{II.5}$$

where σ_T is the standard deviation of the cross-correlation function. Defining ΔT as a time scale satisfying: $R(T+\Delta T) = R_{max}/2$, the standard deviation equals: $\sigma_T = \Delta T/1.175$ for a true Gaussian distribution. The standard deviation of the bubble travel time σ_t is a function of both the standard deviations of the cross-correlation and autocorrelation functions:

$$\sigma_T = \frac{\sqrt{\Delta T^2 - \Delta t^2}}{1.175} \tag{II.6}$$

where Δt is the characteristic time for which the normalised autocorrelation function equals 0.5.

Assuming that $t' \sim T$ and that the bubble/droplet travel distance is a constant Δx, equation (II.4) implies that the turbulence intensity u'/V equals:

$$Tu = \frac{u'}{V} \approx 0.851 \frac{\sqrt{\Delta T^2 - \Delta t^2}}{T} = Tu'. \tag{II.7}$$

Tu' is a dimensionless velocity scale, that is characteristic of the turbulent velocity fluctuations over the distance Δx separating the probe sensors. Although Tu' is not strictly equal to the dimensionless turbulent velocity fluctuation $Tu = u'/V$, the distributions of modified turbulence intensity Tu' provide some qualitative information on the turbulent velocity field in gas-liquid flows.

Kipphan (1977) developed a slightly different reasoning for two-phase mixtures such as pneumatic conveying. He obtained a result of similar form:

$$\frac{u'}{U_w} = \sqrt{\frac{\sigma_T^2 - \sigma_t'^2}{T^2}} \tag{II.8}$$

where U_w is the mean flow velocity, T is the mean particle travel time (e.g. on the conveyor, in the pipe) and σ_t' is the standard deviation of the autocorrelation function. It is believed however that Kipphan's result (equation (II.8)) is not strictly exact ([g]).

[f] For example, affected only by random advective dispersion of the bubbles and random velocity fluctuations over the distance separating the probe sensors

[g] The assumptions of $t' \sim T$ and equation (II.7) are not strictly correct.

Notation

C	air concentration (or void fraction);
C_{mean}	mean void fraction defined in terms of 90%−air content: $C_{mean} = \frac{1}{Y_{90}} \int_0^{Y_{90}} C\, dy$;
D_H	hydraulic diameter (m);
D_0	dimensionless term;
D_t	turbulent diffusivity (m^2/s) of air bubbles in air-water flow;
$D^\#$	dimensionless turbulent diffusivity: $D^\# = D_t/(V_1 d_1)$ for two-dimensional shear flow and $D^\# = D_t/(V_1 r_1)$ for circular jet;
d	1- flow depth (m) measured normal to invert or normal to pseudo-bottom (skimming flow); 2- jet diameter (m);
d_{ab}	air bubble diameter (m);
d_c	critical flow depth (m);
d_1	1- upstream flow depth (m); 2- initial water depth (m);
F	bubble count rate or bubble frequency (Hz) defined as the number of bubbles impacting the probe sensor per second;
Fr	Froude number;
Fr_1	upstream Froude number;
g	gravity acceleration (m/s^2);
H	total head (m);
h	step height (m);
i	integer;
K'	integration constant;
k_s	equivalent roughness height (m);
l	step length (m);
N	number of data;
P	pressure (Pa);
Q	water discharge (m^3/s);
q	water discharge per unit width (m^2/s);
q_{air}	air flux (m^2/s) per unit width;
R	normalised cross-correlation coefficient;
r	radius (m);
r_1	circular jet radius (m) at impact;
T	characteristic bubble travel time (s);
Tu	turbulence intensity defined as: $Tu = u'/V$;
Tu'	modified turbulence intensity in air-water flow (Appendix II);
t	time (s);

u_r	bubble rise velocity (m/s);
u'	root mean square of longitudinal component of turbulent velocity (m/s);
V	velocity (m/s), or air-water velocity in air-water flows;
V_{air}	air velocity (m/s);
V_c	critical flow velocity (m/s);
V_e	onset velocity (m/s) of air entrainment at plunging jet;
V_i	induction trumpet velocity (m/s);
V_1	jet impact velocity (m/s);
v'	normal component of turbulent velocity (m/s);
W	channel width (m);
x	longitudinal distance (m);
x_1	longitudinal distance (m) between nozzle and jet impact;
$Y_{C_{max}}$	transverse location (m) of maximum void fraction;
Y_{90}	characteristic depth (m) where the void fraction is 90%;
y	distance (m) normal to the bed;
α	invert slope with the horizontal;
δ	boundary layer thickness (m);
δ_{al}	thickness (m) of the air sheet set into motion by a high-velocity plunging jet;
μ	dynamic viscosity (Pa.s) of water;
ρ	water density (kg/m^3);
σ	surface tension between air and water (N/m).

References

1. H.O. Anwar, "Self-aerated flows on chutes and spillways - Discussion". J. of Hyd. Engrg., ASCE **120, No. 6**, 778 (1994).
2. F. Bonetto, D. Drew, and R.T. Jr Lahey, "The analysis of a plunging liquid jet - The air entrainment process". Chem. Eng. Comm. **130**, 11 (1994).
3. T. Brattberg and H. Chanson, "Air entrapment and air bubble dispersion at two-dimensional plunging water jets". Chemical Engineering Science **53, No. 24**, 4113 (1998).
4. T. Brattberg and H. Chanson, "Air entrapment and air bubble dispersion at two-dimensional plunging water jets - Errata." Chemical Engineering Science **54, No. 12**, 1925 (1999).
5. T. Brattberg, H. Chanson and L. Toombes, "Experimental investigations of free-surface aeration in the developing flow of two-dimensional water jets". J. of Fluids Eng., Trans. ASME **120, No. 4**, 738 (1998).

6. P. Cain, "Measurements within self-aerated flow on a large spillway". Ph.D. Thesis, Ref. 78-18, Dept. of Civil Engrg., Univ. of Canterbury, Christchurch, New Zealand.
7. H. Chanson, "Self-aerated flows on chutes and spillways". J. of Hyd. Engrg., ASCE **119, No. 2**, 220 (1993).
8. H. Chanson, "Self-aerated flows on chutes and spillways - Discussion". J. of Hyd. Engrg., ASCE **120, No. 6**, 778 (1993).
9. H. Chanson, "Air bubble diffusion in supercritical open channel flow". Proc. 12th Australasian Fluid Mechanics Conference AFMC **2**, 707 (1995).
10. H. Chanson, *Air bubble entrainment in free-surface turbulent shear flows.* Academic Press, London, UK, (1997).
11. H. Chanson, "Air bubble entrainment in open channels. Flow structure and bubble size distributions". Int. J. of Multiphase Flow **23, No. 1**, 193 (1997).
12. H. Chanson, "Le développement historique des cascades et fontaines en gradins". ("Historical development of stepped cascades and fountains".) J La Houille Blanche **7/8**, 76 (1998).
13. H. Chanson, "Turbulent open-channel flows: drop-generation and self-aeration. Discussion". J. of Hyd. Engrg., ASCE **125, No. 6**, 668 (1999).
14. H. Chanson, S. Aoki, and M. Maruyama, "Air bubble entrainment at plunging breakers and its effect on long period waves: an experimental study". Coastal/Ocean Engineering Report, No. COE99-1, Dept. of Architecture and Civil Eng., Toyohashi University of Technology, Japan, July, 41 pages. (1999)
15. H. Chanson, S. Aoki, and M. Maruyama, "Unsteady air bubble entrainment at a plunging breaker: a full-scale modelling". Book of Abstracts - EUROMECH Colloquium, N.416 , 47 (2000).
16. H. Chanson, and T. Brattberg, "Air entrainment by two-dimensional plunging jets: the impingement region and the very-near flow field". Proc. 1998 ASME Fluids Eng. Conf , Paper FEDSM98-4806, (CD-ROM) (1998).
17. C. Crowe, M. Sommerfield and Y. Tsuji, *Multiphase flows with droplets and particles.* CRC Press, Boca Raton, USA, (1998).
18. P.D. Cummings and H. Chanson, "Air entrainment in the developing flow region of plunging jets. Part 1: Theoretical development." J. of Fluids Eng., Trans. ASME **119, No. 3**, 597 (1997).
19. P.D. Cummings and H. Chanson, "Air entrainment in the developing flow region of plunging jets. Part 2: Experimental." J. of Fluids Eng., Trans.

ASME **119, No. 3**, 603 (1997).
20. P.D. Cummings, P.D. and H. Chanson, "An experimental study of individual air bubble entrainment at a planar plunging jet." Chem. Eng. Research and Design, Trans. IChemE, Part A **77, No. A2**, 159 (1999).
21. R. Ehrenberger, "Wasserbewegung in steilen rinnen (Susstennen) mit besonderer berucksichtigung der selbstbelüftung." ("Flow of water in steep chutes with special reference to self-aeration.") Zeitschrift des österreichischer Ingenieur und Architektverein, No. 15/16 and 17/18 (in German) (translated by Wilsey, E.F., U.S. Bureau of Reclamation).
22. M. El-Hammoumi, "Entrainement d'air par jet plongeant vertical. Application aux becs de remplissage pour le dosage pondéral." ("Air entrainment by vertical plunging jet. Application to refill nozzles applied to dosage."). Ph.D. thesis, INPG, Grenoble, France (in French).
23. D.A. Ervine and H.T. Falvey, "Behaviour of turbulent water jets in the atmosphere and in plunge pools." Proc. Instn Civ. Engrs., Part 2 **83**, 295 (1987).
24. D.A. Ervine and H.T. Falvey, "Behaviour of turbulent water jets in the atmosphere and in plunge pools Discussion." Proc. Instn Civ. Engrs., Part 2 **85**, 359 (1987).
25. D.A. Ervine, E.J. McKeogh and E.M. Elsawy, "Effect of turbulence intensity on the rate of air entrainment by plunging water jets." Proc. Instn Civ. Engrs, Part 2 , 425 (1980).
26. A. Fuhrboter, "Air entrainment and energy dissipation in breakers." Proc. 22nd Int. Conf. Coastal Eng. - ASCE , 391 (1970).
27. G.H. Keulegan and G.W. Patterson, "Mathematical theory of irrotational translation waves." J. of Research of the Nat. Bureau of Standards, RP1273, US Dept. of Commerce **24, No. 1**, 47 (1940).
28. H. Kipphan, "Bestimmung von tranportkenngröβen bei Mehrphasenströmungen mit hilfe der korrelationsmeβtechnik (in German)." Chemie Ingenieur Technik **49, No. 9**, 695 (1977).
29. A.M. Lezzi and A. Prosperetti, "The stability of an air film in a liquid flow." J. Fluid Mech. **226**, 319 (1991).
30. E.J. McKeogh, "A study of air entrainment using plunging water jets." Ph.D. thesis, Queen's University of Belfast, UK, (1978).
31. R. Manasseh and H. Chanson, "Void-fraction and acoustic characteristics of gas bubbles entrained by a circular plunging jet." Proc. 4th Intl Conf. Multiphase Flow, ICMF'01 , Ref. 347 (CD-ROM) (2001).
32. G. Plumptre, *The water garden.* Thames and Hudson, London, UK, (1993).
33. M. Rein, "Turbulent open-channel flows: drop-generation and self-aeration." J. of Hyd. Engrg., ASCE **124, No.1**, 98 (1998).
34. M. Rein, "Turbulent open-channel flows: drop-generation and self-aeration Discussion." J. of Hyd. Engrg., ASCE **125, No.6**, 668 (1998).
35. H. Schlichting, *Boundary layer theory.* McGraw-Hill, New York, USA, 7th edition, (1979.
36. M.R. Spiegel, *Mathematical handbook of formulas and tables.* McGraw-Hill Inc., New York, USA, (1974).
37. L.G. Straub and A.G. Anderson, "Experiments on self-aerated flow in open channels." J. of Hyd. Div., Proc. ASCE **84, No. HY7**, 1890-1 (1958).
38. L. Toombes, L. "Experimental study of air-water flow properties on low-gradient stepped cascades." Ph.D. thesis, Dept of Civil Engineering, University of Queensland, Brisbane, Australia, (2002).
39. M.P. Tulin and T. Waseda, "Laboratory observations of wave group evolution, including breaking effects." J. Fluid Mech. **378**, 197 (1999).
40. E. Van de Sande and J.M. Smith, "Surface entrainment of air by high velocity water jets." Chem. Eng. Science **28**, 1161 (1973).
41. I.R. Wood, *Air entrainment in free-surface flows.* IAHR Hydraulic Structures Design Manual No. 4, Hydraulic Design Considerations, Balkema Publ., Rotterdam, The Netherlands, (1991).
42. Y.G. Zhu, H.N. Oguz and A. Prosperetti, "Mechanism of Air entrainment by an Impinging Liquid Jet." Proc. 13th Australasian Fluid Mech. Conf. **1**, 337 (1998).

Internet resources

General resources

`Gallery of photographs`	`www.uq.edu.au/~e2hchans/photo.html`
`Reprints of research papers`	`www.uq.edu.au/~e2hchans/reprints.html`
`NASA Earth observatory`	`earthobservatory.nasa.gov/`
`The formal water garden`	`www.uq.edu.au/~e2hchans/wat_gard.html`

Air entrainment in plunging jet

`Air entrainment in the developing flow region of plunging jets - Databank`	`www.uq.edu.au/~e2hchans/data/jfe97.html`

Air entrainment at a circular plunging jet: physical and acoustic characteristics - Internet Database	www.uq.edu.au/~e2hchans/bubble/
Research papers in plunging jet flows	www.uq.edu.au/~e2hchans/reprints.html#journal

Air entrainment in stepped cascades

Photograph of stepped spillways	www.uq.edu.au/~e2hchans/photo.html#Step_spillways
Self-aeration down smooth and stepped chutes	www.uq.edu.au/~e2hchans/self_aer.html
Research papers in stepped chute flows	www.uq.edu.au/~e2hchans/reprints.html#journal

Air-sea mass transfer

NASA rain, wind and air-sea gas exchange research	bliven2.wff.nasa.gov/index.ht
Northern hemisphere sensitivity to sea surface temperature change	www.giss.nasa.gov/research/paleo/sst/

THE DYNAMICS OF STRONG TURBULENCE AT FREE SURFACES. PART 2. FREE-SURFACE BOUNDARY CONDITIONS

M. BROCCHINI
D.I.Am., Università di Genova,
16145 Genova, Italy

D.H. PEREGRINE
School of Mathematics, University of Bristol,
Bristol, BS8 1TW, U.K.

Strong turbulence at a water–air free surface can lead to splashing and a disconnected surface as in a breaking wave. Averaging to obtain boundary conditions for such flows first requires equations of motion for the two-phase region. These are derived using an integral method, then averaged conservation equations for mass and momentum are obtained along with an equation for the turbulent kinetic energy in which extra work terms appear. These extra terms include both the mean pressure and the mean rate of strain and have similarities to those for a compressible fluid. Boundary conditions appropriate for use with averaged equations in the body of the of the water are obtained by integrating across the two-phase surface layer.

A number of 'new' terms arise for which closure expressions must be found for practical use. Our knowledge of the properties of strong turbulence at a free surface is insufficient to make such closures. However, preliminary discussions are given for two simplified cases in order to stimulate further experimental and theoretical studies.

Much of the turbulence in a spilling breaker originates from the foot of the breaker where turbulent water meets undisturbed water. A discussion of averaging at the foot of a breaker gives parameters that may serve to measure the 'strength' of a breaker.

1 Introduction

In Part 1 (Brocchini and Peregrine 2001) the effects of strong turbulence at a free surface are described, and a semi-quantitative classification introduced. Part 2 is also motivated by a wish to improve modelling of breaking water waves, but the analysis is applicable to the wider range of flows described in Part 1. We approach the problem from the standard Reynolds averaging of the equations of motion of a turbulent fluid. The two-phase nature of the

ADVANCES IN COASTAL AND OCEAN ENGINEERING

Interaction of Strong Turbulence with Free Surfaces

Volume 8

Guest Editors

M. Brocchini
University of Genova, Italy

D. H. Peregrine
University of Bristol, UK

Editor

Philip L.-F. Liu
Cornell University, USA

World Scientific
New Jersey • Singapore • London • Hong Kong

Published by

World Scientific Publishing Co. Pte. Ltd.
P O Box 128, Farrer Road, Singapore 912805
USA office: Suite 1B, 1060 Main Street, River Edge, NJ 07661
UK office: 57 Shelton Street, Covent Garden, London WC2H 9HE

British Library Cataloguing-in-Publication Data
A catalogue record for this book is available from the British Library.

ADVANCES IN COASTAL AND OCEAN ENGINEERING, Volume 8

ISBN 981-02-4952-7

Printed in Singapore by World Scientific Printers

PREFACE TO THE REVIEW SERIES

The rapid flow of new literature has confronted scientists and engineers of all branches with a very acute dilemma: How to keep up with new knowledge without becoming too narrowly specialized. Collections of review articles covering broad sectors of science and engineering are still the best way of sifting new knowledge critically. Comprehensive review articles written by discerning scientists and engineers not only separate lasting knowledge from the ephemeral, but also serve as guides to the literature and as stimuli to thought and to future research.

The aim of this review series is to present critical commentaries of the state-of-the-art knowledge in the field of coastal and ocean engineering. Each article will review and illuminate the development of scientific understanding of a specific engineering topic. Our plans for this series include articles on sediment transport, ocean waves, coastal and offshore structures, air-sea interactions, engineering materials, and seafloor dynamics. Critical reviews on engineering designs and practices in different countries will also be included.

P. L.-F. Liu